Initial Shakedown Testing of the Stevens Shock Tunnel

D. Shekhtman*, A. Hameed†, B. A. Segall‡, A. R. Dworzanczyk§, and N. J. Parziale¶
Stevens Institute of Technology, Hoboken, NJ 07030, USA

The Stevens Shock Tunnel is designed to replicate hypersonic, Mach 6 flow conditions. The tunnel produces a core flow of 0.3 m in the test section and a test time of at least 4 ms. This paper describes the tunnel's operation and flow characterization for a range of run conditions: Mach 5.8-6.0, enthalpy 1.5 MJ/Kg, and unit Reynolds number 0.35-8.1×10^6 1/m (with a potentially lower limit available). This paper also describes the use of a nozzle centerbody flow terminator and debris blocker and tunnel cleaning to remove residual debris from a previous experiment. Reservoir, static, and Pitot pressure measurements are presented for a range of run conditions and compared to nozzle flow calculations.

Nomenclature

P_1 = Driven Section Pressure, (Pa)
P_4 = Driver Section Pressure, (Pa)
P_r = Reservoir Pressure, (Pa)
h_r = Reservoir Enthalpy, (MJ/kg)
T_r = Reservoir Temperature, (K)
u_s = Shock Speed, (m/s)
Region 1 = Driven Section
Region 2 = Incident Shock-Processed Region
Region 4 = Driver Section
Region 5s = Nozzle Reservoir (Reflect-Shock-Processed Region)

I. Introduction

Hypersonic vehicle design requires an understanding of flow phenomena to (a) predict flow features (separation bubbles, wakes, transition, etc.) and (b) calculate engineering quantities (i.e. lift, drag, wall temperature). Due to short timescales in hypersonic flow, impulse facilities with millisecond test times can be sufficient for the research of canonical flows and hypersonic vehicle design. Shock tunnels are typically used to replicate the enthalpy of free-flight and Earth re-entry. Some large-scale reflected-shock tunnels include NASA HYPULSE [1], Caltech T5 [2], High Energy Shock Tunnel Göttingen (HEG) [3], and the CUBRC LENS tunnels [4, 5]. In some of these shock-tunnels, bifurcation at high driver-to-driven pressure ratios is noted, and the LENS tunnel by design required additional measures to deal with over-pressure of the test section and dump tank [4–6].

Chu et al. [1] observed and analyzed bifurcation in the NASA HYPULSE facility at GASL. They showed that inside the nozzle reservoir, the driver-gas makes its way towards the nozzle centerline in the form of a finger-like jetting structure. Their proposal to alleviate driver-gas contamination effects was the installation of a sleeve in the nozzle reservoir that is concentric with the driven tube*. In the Caltech T5 piston-driven reflected-shock tunnel, Sudani et al. [7, 8] implemented a reservoir sleeve to block the driver-gas "finger" from contaminating the center of the nozzle flow. Their design also incorporated a concentric reservoir to store driver gas during a run. They reported success in increasing the usable test time prior to bifurcation. Hannemann et al. [3] at HEG also implemented a nozzle sleeve in a piston-driven shock tunnel. However, their design did not use a separate, dedicated driver gas reservoir. Instead, the

---

*Graduate Student, Mechanical Engineering, Castle Point on Hudson, Hoboken, New Jersey, 07030.
†Graduate Student, Mechanical Engineering, Castle Point on Hudson, Hoboken, New Jersey, 07030.
‡Graduate Student, Mechanical Engineering, Castle Point on Hudson, Hoboken, New Jersey, 07030.
§Graduate Student, Mechanical Engineering, Castle Point on Hudson, Hoboken, New Jersey, 07030.
¶Associate Professor, Mechanical Engineering, Castle Point on Hudson, Hoboken, New Jersey, 07030, AIAA Senior Member.
*This solution is still a work-in-progress in our lab.

sleeve was conveniently mounted to the end cap of a nozzle cap. The small annular volume between the driven-tube wall and the sleeve was used to contain driver-gas jetting during a run. They also reported an increase of approximately 100% in usable test time.

At the CUBRC LENS tunnel, steps were taken to prevent nozzle recoil and dump-tank over-pressure. Holden et al. [9] states that the CUBRC LENS tunnel has a centerbody nozzle flow terminator and a relief tank equipped with a pressure-relief valve in a separate outside space. Under normal operation, the centerbody apparatus functions as a fast-acting plug valve. It blocks nozzle flow once the useful test gas slug has been depleted in the reservoir, thus ending the tunnel run. By not allowing driver gas to pass through the nozzle, LENS can reduce nozzle recoil in addition to preventing over-pressure of the dump tank. Additionally, the centerbody acts as a debris blocker, protecting the surfaces of test articles in the test section.

In the Stevens Shock Tunnel, multiple strategies were employed to prevent the premature driver gas contamination in the nozzle reservoir. These included honing the driven section pipes, extending the length of the driven section, changing primary diaphragm station location, shock tunnel cleaning, and even installing a nozzle centerbody (to act as both a flow terminator and diaphragm debris blocker). Their effectiveness is measured via the steadiness of nozzle rake Pitot probes and static pressure probes and compared to nozzle calculations.

II. Facility: The Stevens Shock Tunnel

The Stevens Shock Tunnel is a facility designed to replicate Mach 6 free-flight flow conditions with an enthalpy of 1.5 MJ/kg and a unit Reynolds number $0.35 - 8.1 \times 10^6$ m^{-1} for at least 4 ms. The construction of the shock tunnel obeys ASME standard B16.5 Pipe Flanges and Flanged Fittings for flanges and olets [10] and ASME standard B31.1 Power Piping for all pipes [11]. The tunnel consists of off-the-shelf components, some of which were modified with O-ring grooves. Class 900, size 8 piping was used for the driver and driven sections, and class 150 was used for the dump tank flanges. All welds were full-penetration in accordance with the standards. As determined by the standards and by hydrotesting, the maximum allowable pressure of the straight portions of the driver and driven sections is 16.6 MPa (2400 psig) and the maximum allowable pressure of the elbow is 10.4 MPa (1500 psig). In Fig. 1, the current configuration of the tunnel is displayed. The driver section is 5.0 m long, and the driven section is 11.07 m long. Up to 5 transducer stations are used to provide a shock-speed measurement. Pressure transducers are flush with the pipe. The nozzle reservoir pressure is measured 0.0254 m (1 inch) from the shock tube end. The test section has an inner diameter of 0.610 m (24 in) and is large enough to accommodate a 34-36° hollow-cylinder flare of 0.203 m (8 in) diameter without tunnel startup issues (see Appendix A). The dump tanks can hold a volume of 8.78 m^3 (2320 gal) at a vacuum pressure of 350 mtorr and have a maximum rated pressure of 40 psig. Helium is typically used as the driver gas, and, for these shakedown tests, lab air is used for the test gas. To sustain the recoil of the facility, the driver section, driven section, and nozzle rest on Standon pipe supports mounted onto Nippon bearing carriages and rails, which are fastened to steel tables.
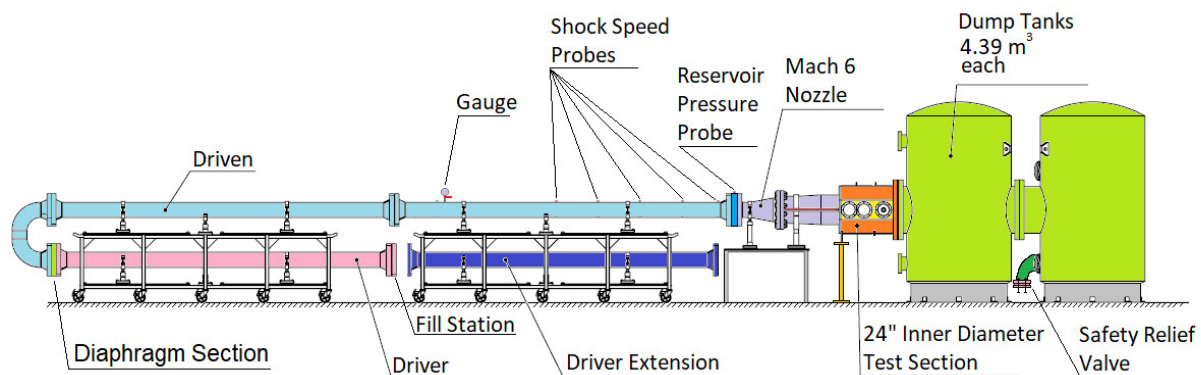
Fig. 1   Schematic of Stevens Shock Tunnel (SST).
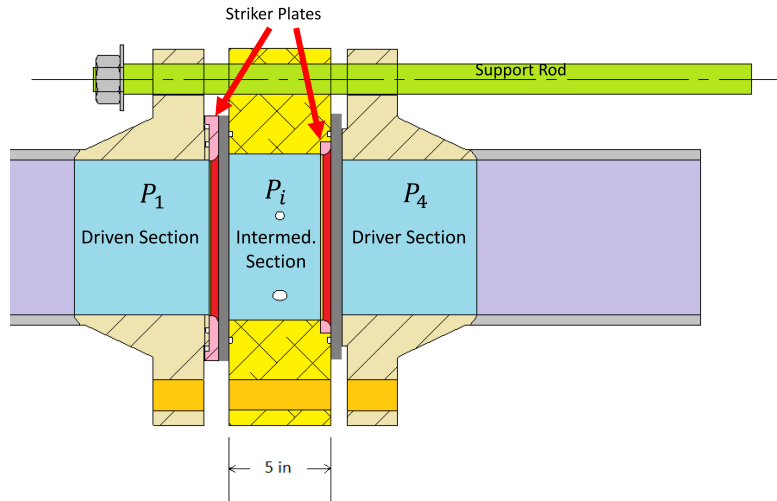
Fig. 2   Double Diaphragm Section in the Bottom Diaphragm Station, before the Elbow, as depicted in Fig. 1.

Table 1   Max Pressure Differential vs. Diaphragm Thickness for Temper O aluminum. For all diaphragms, pressure acts on a diameter of 194 mm (7.625 in).

Grade	Thickness (in)	Unscored, ΔP (psi)	Scored 0.010 in, ΔP (psi)
1100	0.020	103 ± 1	N/A
1100	0.032	171 ± 7	N/A
1100	0.050	280 ± 3	N/A
1100	0.090	495 ± 2	377
1100	0.125	665	550
6061	0.125	956 ± 5	670 ± 60
1100	0.190	≈ 1045	> 750

A. Firing Mechanisms and Diaphragm Material

The pressure rupture of either a single or double diaphragm initiates a run in the Stevens Shock Tunnel. Single-diaphragm rupture is used for prototyping runs. As shown in Fig. 2, a double diaphragm mechanism [12] is used to conduct high pressure runs at specified pressures and pressure ratios ($P_4 > 1.03$ MPa (150 psia)).[†]

Typical diaphragms consist of standard square 12 in × 12 in 1100-O aluminum of different thicknesses ranging between 0.010 to 0.190 inches. Burst pressures for such diaphragms with fixed-end boundary conditions are listed in Table 1. We observed that soft Temper O aluminum and cold-rolled steel were more effective in petalling than harder materials, which tended to shatter during rupture. Clamping of the diaphragm is achieved by (a) twelve 1-3/8-6 Grade 5 bolts torqued to 340-420 lbf·ft and (b) concentric serrations on the ASME B16.5 Class 900 Flanges that prevent the slippage of diaphragm material relative to the flange. Fixed ends constrain a diaphragm to thin out at the center instead of the ends. Flange serrations are critical to this effect. According to Gaydon et al. [12, Ch. 5], friction generated by bolt torque is generally insufficient as a sole means to enforce the fixed-ends constraint. A striker plate, as shown in Fig. 2, is used to form a bend radius at the edge of each diaphragm as it bulges into a dome via applied pressure. Diaphragm scoring is used to encourage petalling of diaphragms and to improve pressure recovery P_R/P_4. Scoring to a depth of 0.010 in is accomplished via CNC machining. A stamp is currently being tested to eliminate the need to machine an X on the diaphragms.

[†]Meanwhile, a pneumatic plunger mechanism, which has seen limited use in shock tube tests, is intended for use in low-to-medium pressure experiments ($P_4 < 3.45$ MPa (500 psia)).

3

Table 2   Run Conditions, where P_4 is Driver-section helium pressure; P_4/P_1 is the driver-to-driven pressure ratio that determines the driven air pressure P_1; u_s is the shock speed; M_s is the shock Mach number; T_r is the reservoir temperature; P_r is the reservoir pressure; h_r is the reservoir enthalpy; and Y/N denote yes or no, respectively. D. Loc. stands for diaphragm location (T for top after elbow and B for bottom before elbow); the ball column indicates the use of a centerbody; and the DD column indicates the use of a double diaphragm firing mechanism. NA stands for not available. All shots except Shot 173 used a He driver. Shot 173 used a 50% N_2:50% He driver.

Shot	P_4 (MPa)	$\dfrac{P_4}{P_1}$	$\dfrac{P_R}{P_4}$	u_s (m/s)	M_s	P_R (MPa)	T_r (K)	h_r (MJ/kg)	M_∞	Re_∞ 10^6 (1/m)	Ball	D. Loc.	DD
169	3.58	114	0.74	1220	3.51	2.67	1670	1.57	5.83	3.0	Y	B	N
171	3.38	107	0.80	1200	3.44	2.72	1650	1.54	5.90	NA	Y	T	N
173	0.88	5	0.90	500	1.44	0.79	470	0.17	5.87	7.0	Y	B	N
179	3.93	125	0.74	1240	3.58	2.93	1740	1.66	5.60	NA	N	B	N
180	1.21	120	0.71	1200	3.44	0.859	1650	1.54	6.05	0.94	Y	B	Y
181	3.47	121	0.69	1220	3.51	2.40	1670	1.56	5.89	NA	Y	B	Y
182	5.29	115	0.71	1220	3.77	2.40	1660	1.56	5.83	NA	Y	B	Y
183	6.99	115	0.73	1200	3.44	5.09	1640	1.53	5.94	5.3	Y	B	Y
184	7.03	111	0.74	1200	3.44	5.17	1630	1.51	5.84	5.6	Y	B	Y
185	8.26	110	0.74	1220	3.51	6.11	1660	1.51	5.80	6.4	Y	B	Y
189	10.4	110	N/A	1220	3.51	N/A	N/A	N/A	5.85	N/A	Y	B	Y
190	10.3	110	0.73	1200	3.44	7.52	1620	1.51	5.75	8.14	Y	B	Y
192	0.45	110	0.73	1220	3.51	0.326	1650	1.54	5.95	0.35	Y	B	Y

III. Shakedown Testing of Stevens Shock Tunnel

   A variety of different configurations and setups were attempted in the Stevens Shock Tunnel to optimize operation. Fig. 1 shows the current setup of the tunnel with a long driven section (11 m) and the diaphragm station in the bottom before the elbow. A rake with 12 pitot probes was mounted to capture the axial flow profile of the nozzle. Two static pressure probes were mounted: one 67.56 mm (2.66 in) from the centerline of the nozzle to obtain centerline pressure and the other 76 mm (3 in) above the nozzle wall. Run conditions are listed in Table 2. Reservoir Conditions were calculated in MATLAB using Cantera [13] with the Shock and Detonation Toolbox [14]. The appropriate thermodynamic data are found in the literature [15, 16].

   In Fig. 3, shots 180-185 and 189 were conducted with a double diaphragm firing mechanism and a neoprene ball centerbody (see Fig. 6) at a pressure ratio P_4/P_1 range of 110-121, corresponding to a reservoir enthalpy H_R range of 1.51-1.56 MJ/kg. For a range of driver pressures $1.21 \leq P_4 \leq 8.26$ MPa (175-1200 psia), the reservoir pressure P_R was sufficiently tailored at 0.859-6.11 MPa and the reservoir temperature was $1630 - 1660$ K. For shots 180-190, the nozzle generated Mach 5.8-6.0 flow with a unit Reynolds number between $0.94-8.1 \times 10^6$ 1/m and a static pressure of 0.053-3.62 kPa (0.0076-0.53 psi).

   Fig. 3 shows pressure traces with no evidence of driver gas contamination, which we believe to be indicated by the onset of large oscillations in the Pitot probe traces (see Figs. 7 and 8 for examples). Fig. 4 demonstrates that the core flow has a diameter of at least 300 mm (11.8 in). Numerical nozzle flow solutions were obtained via the University of Minnesota Nozzle Code (known also as the Data Parallel Line Relaxation (DPLR) computational fluid dynamics code) [17]. The measured static pressure, Pitot-pressure profile, and the Mach number agree well with the computed laminar nozzle calculations; but, the laminar calculation does not predict the shear-layer width. If a turbulent flow solution is calculated with DPLR, the static and Pitot pressures are over-predicted by approximately 5%, but the larger shear layers are captured. Because we are only interested in the mean value of the core flow, we will use the laminar conditions for the run-condition calculation for this paper and examine alternate turbulence models in the future.

(a) Shot 181

(b) Shot 183

(c) Shot 185

(d) Shot 190
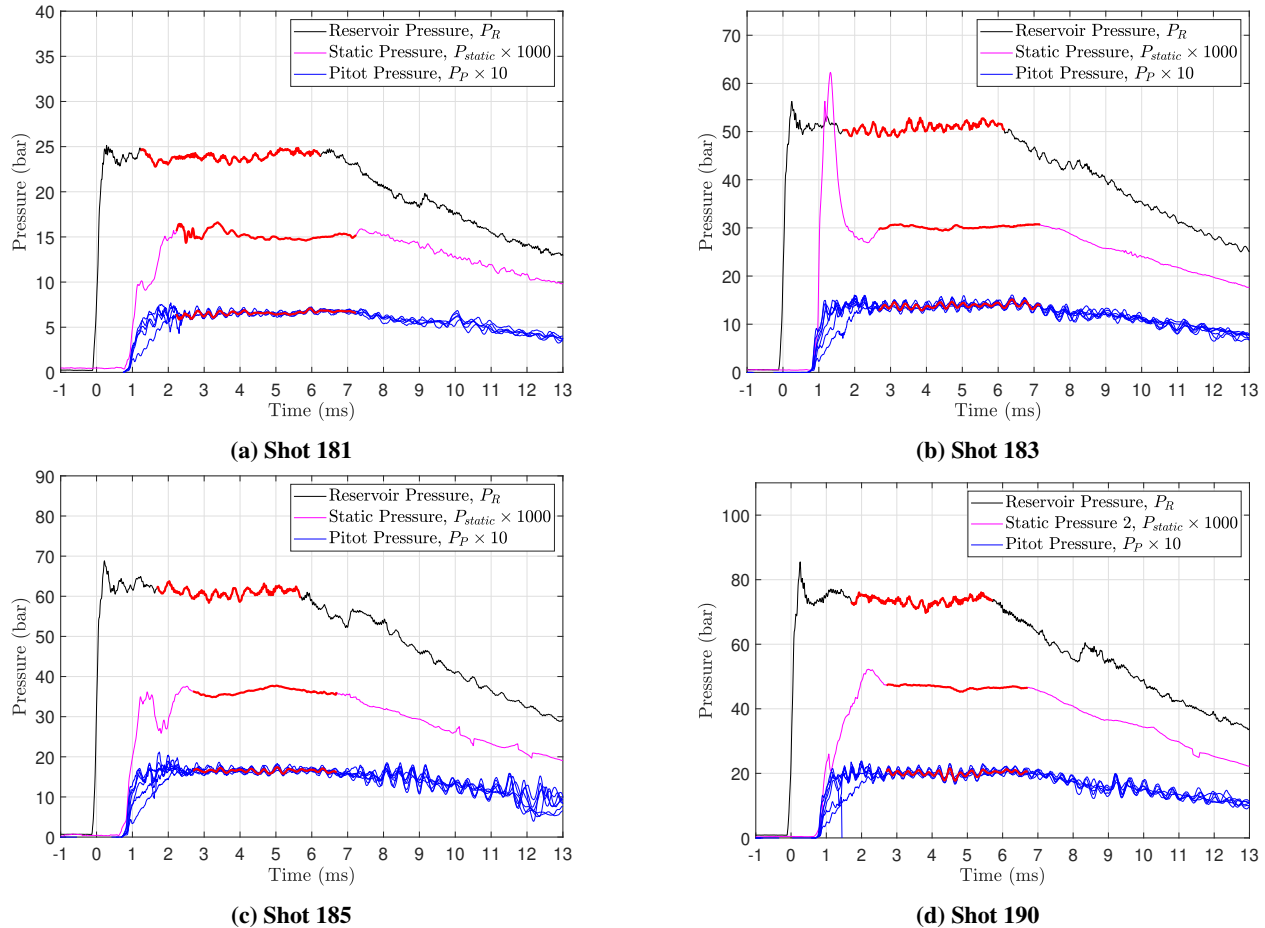
Fig. 3   Shock Tunnel Pressure Traces for Shock Tunnel Run Initiated by a Double Diaphragm Firing Mechanism. Note that pitot probes shown lie within the nozzle core flow. The red overline represents usable test time.

IV. Centerbody Design

Premature arrival of driver gas in the reservoir region would manifest as large oscillations in Pitot-pressure traces, a bump in the center of the Pitot-pressure profile, and potentially, altering the test-gas composition (as shown in Fig. 12 at 5.5 ms). The causes of this early, nonuniform reservoir contamination likely includes bifurcation. According to Davies [18] and Davies et al. [19], when helium gas drives nitrogen test gas, bifurcation occurs when the incident shock Mach number is greater than 3.5, which unfortunately is near the run condition (listed in Table 2) for generating tunnel's design enthalpy. From [1, 20], wall-jetting due to bifurcation forms a finger-like structure that contaminates the centerline of the nozzle exit flow. Following the strategy of Holden *et al.* and CUBRC [4, 9] for the CUBRC Shock Tunnel, a simplified implementation of a centerbody apparatus was installed in the reservoir section of the Stevens Shock Tunnel to terminate nozzle flow once the useful test gas slug has been depleted. As shown in Fig. 6, a neoprene ball was placed 16 mm (0.63 inches) from the reservoir region. During a shock tunnel run, driven and driver gas push the ball approximately 36 mm (1.415 in) towards the nozzle converging section. The ball's motion is depicted sequentially in Figs. 6a and 6b.

The neoprene ball centerbody fulfills three major functions. It (1) prevents diaphragm debris from entering the nozzle, (2) shields the nozzle, and (3) blocks premature arrival of driver gas along the tunnel centerline. As demonstrated by Fig. 7, the neoprene ball is one major factor in the generation of smooth Pitot and static pressure traces. It prevents driver gas contamination from occurring within the test time at $t = 7$ ms. Additionally, if the ball properly seals during a run, nozzle recoil and structural loading are significantly reduced; and potentially, driver gas remaining in the tube can be piped out and reused. Efforts to reliably seal with the ball centerbody are still ongoing, bearing in mind that the ball's center should be initially along the centerline of the nozzle.

5

(a) Shot 169

(b) Shot 183

(c) Shot 185

fill

(d) Shot 190
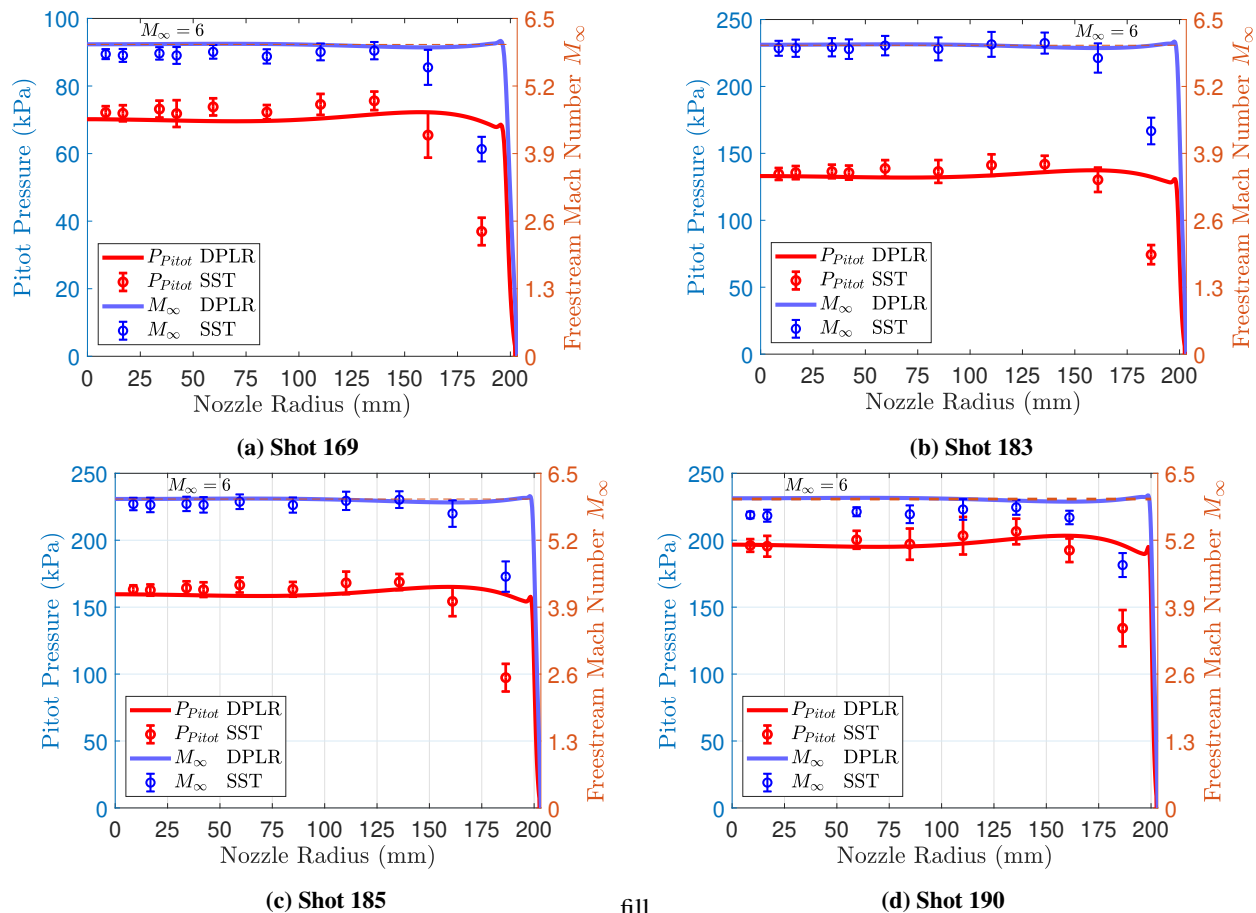
Fig. 4   Shock Tunnel Pressure Traces for Shock Tunnel Run Initiated by a Double Diaphragm Firing Mechanism. Note that pitot probes shown lie within the nozzle core flow.

In the Pitot-pressure traces in Fig. 8, the location of the diaphragm station (top or bottom of elbow) also plays a role in preventing driver gas contamination from taking place during the test time. With the diaphragm located at the top of the elbow, the reservoir pressure trace is steady for a longer period, but the test slug is smaller, so the usable test time is shorter. With the diaphragm station located at the bottom of the elbow, the expansion fan terminates the test time, not the onset of large flow oscillations.

However, when the ball is used in conjunction with the diaphragm station placed below before the elbow, pressures traces like those obtained during Shot 169 become routine in the SST, as demonstrated in Figs. 3 and 4. When considering the deployment of test articles in the test section of the SST, start-up time must be subtracted from usable test time. Therefore, from Fig. 12 in appendix A, the unwanted growth of the separation bubble, due to driver gas contamination, can be delayed by 2 ms, resulting a longer, usable test time beyond 5.86 ms, as shown by traces for Run 156, available upon request.

V. Effect of Tunnel Cleanliness

The discussion on the location of the diaphragm station and the use of the ball as a debris blocker extends into shock tunnel cleanliness. Diaphragm ruptures and dump-tank dust clouds deposit material throughout the shock tunnel. Cleaning is essential to protect the integrity of the contact surface during a test and to reduce the amount of debris passing past the ball into the test section. Using the motorized cart presented in Fig. 9 to push out large debris and lay a line through the driven section in Fig. 1, a foam bucket with microfiber cloths is pulled through, collecting dust and small debris. In Fig. 10, the effect of tunnel cleanliness manifests as the amount of diaphragm debris prevented from flying into the test section. Shot 128 is a control shot with no implemented cleaning strategy. Shot 179 is a

6
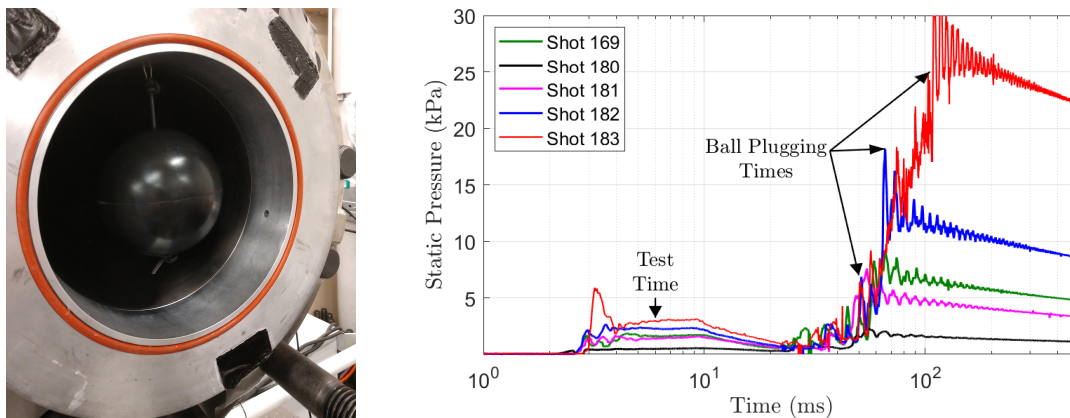
Fig. 5 Nozzle Centerbody. *Left:* **Picture of Nozzle Centerbody.** *Right:* **Static Pressure Traces for Multiple Shots Showing Test Intervals and Ball-Plugging Times.**

(a) Ball Start Position

(b) Ball Final Position
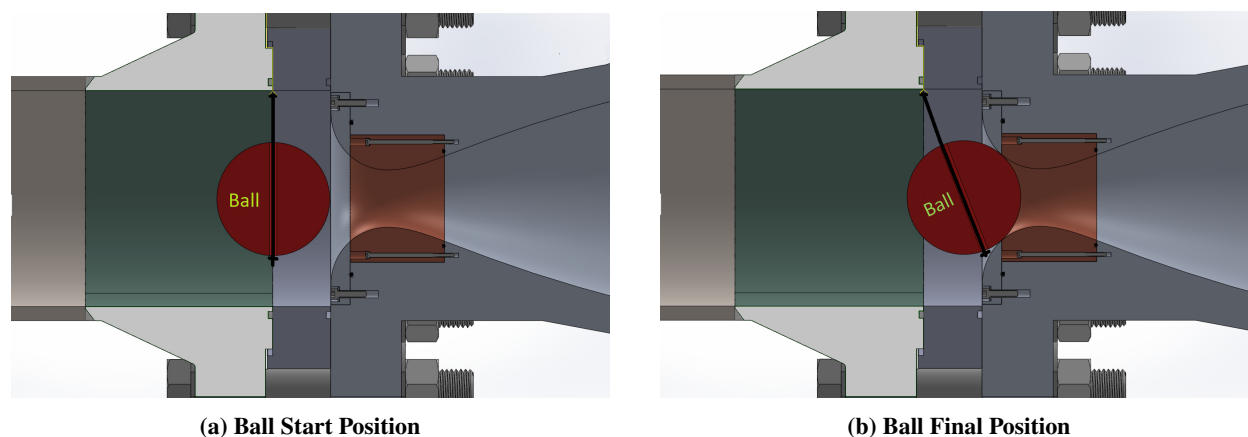
Fig. 6 Schematic of Ball Plugging the Nozzle Converging Section. The ball moves a distance of 35.8 mm (1.41 in) from positions (a) to (b).

shot that uses driven tube cleaning, without a nozzle centerbody (the ball). Shot 157 shows that the ball centerbody and tunnel cleaning are effective in keeping the test section clean during the test time. It is noted that schlieren was unable to indicate the presence of small particulate in the test section. Images were obtained via a Phantom Camera at 20 kHz framerate aimed at the test section window with a Nikon NIKKOR 24–85-mm f/2.8-4D. Maintaining tunnel cleanliness preserves the surface integrity of test articles and the prevents premature transition to turbulence on test articles by diaphragm debris. This adds further sustainability to the test article surface (including coatings such as pressure-sensitive and temperature-sensitive paints [21]) and contributes to the integrity of turbulence experiments, as emphasized by the work of Jewell et al. [22].

VI. Extending Usable Test Time and Increasing Reynolds Number via N_2:He Driver

By using a 50% N_2/50% He Driver with $P_4/P_1 = 5$, the run time can be approximately tripled to 15 ms, and the unit Reynolds number 7×10^6 1/m is achieved in exchange for a reduced enthalpy of 0.17 MJ/kg. The run conditions for this shot, run 173, are detailed in Table 2. The driver gas mixture was prepared in a pressurized tank and left idle for two days. A 50% N_2/50% He Driver with $P_4/P_1 = 5$ is a compromise in required driver pressure P_4 (0.88 MPa vs ≈8.3 MPa) and generated reservoir enthalpy (0.17 MJ/kg vs. 1.5 MJ/kg) for a larger Reynolds number and test time. The extended test time and increased Reynolds number can be used towards turbulence experiments and models which have longer start-up times.
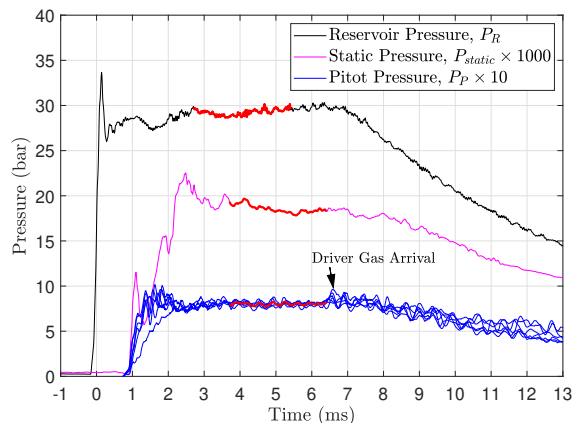
(a) Shot 179: No Ball
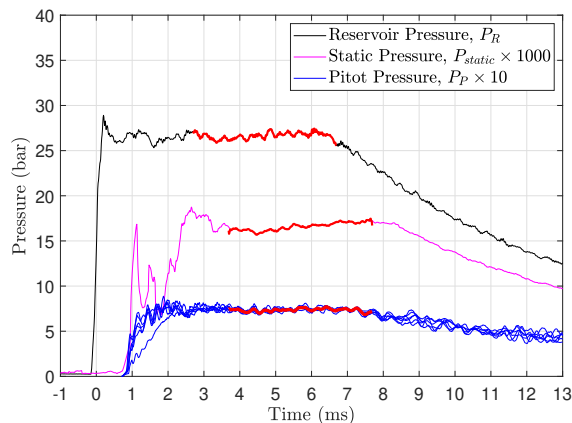
(b) Shot 169: With Ball

Fig. 7   Shock Tunnel Pressure Traces (a) with and (b) without a ball centerbody, shown in Fig. 6. Note that pitot probes shown lie within the nozzle core flow.
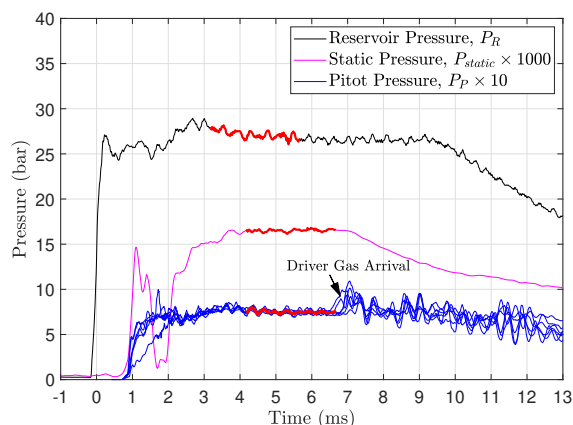
(a) Shot 171: Top Diaphragm Station
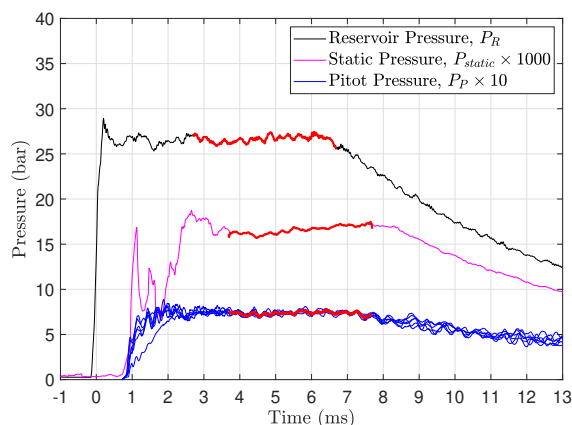
(b) Shot 169: Bottom Diaphragm Station

Fig. 8   Shock Tunnel Pressure Traces with two Different Diaphragm Locations: (a) after elbow and (b) before elbow, as shown in Fig. 1. Note that pitot probes shown lie within the nozzle core flow.

VII. Conclusions

Steady pitot and static pressure traces are presented for experiments over a range of unit Reynolds number (0.35-8.1×10^6 1/m) at Mach 5.8-6.0 and enthalpy 1.54 MJ/kg. By preventing or delaying the premature arrival of driver gas by using a nozzle centerbody and a diaphragm station before the elbow, usable test time is maximized up to the arrival of the expansion fan. Additionally, diaphragm debris was prevented from entering the test section via the nozzle centerbody. Tunnel cleanliness also played an important role in configuring the Stevens Shock Tunnel for transition and turbulence experiments. By reducing the debris output of the nozzle, the surfaces of test articles in the test section are protected. The success of the ball centerbody raises new questions and research opportunities in the Stevens Shock Tunnel.

Appendix A: Driver-Gas Contamination Detection via Schlieren Imaging of a 36° Hollow-Cylinder Flare

This section shows the size of the separation bubble over a hollow-cylinder flare in Fig. 12 can be used to confirm the presence of driver gas contamination for shot 106, when nozzle probes are unavailable. A table of run conditions for shot 106 is provided in Table 3.

8
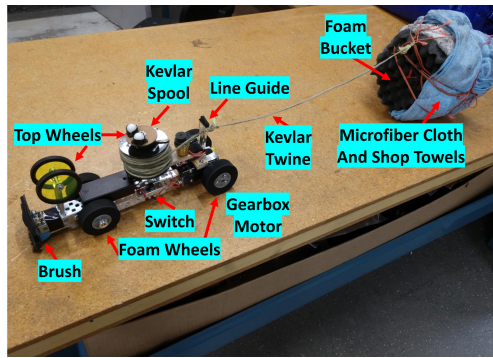
Fig. 9   Motorized Twine-laying Cart and Microfiber Cloth bucket for Stevens Shock Tunnel.

Shot 128
No Ball
No Cleaning

Shot 179
No Ball
W/ Cleaning

Shot 157
W/ Ball
W/ Cleaning

t = 5 ms   t = 6 ms   t = 8 ms
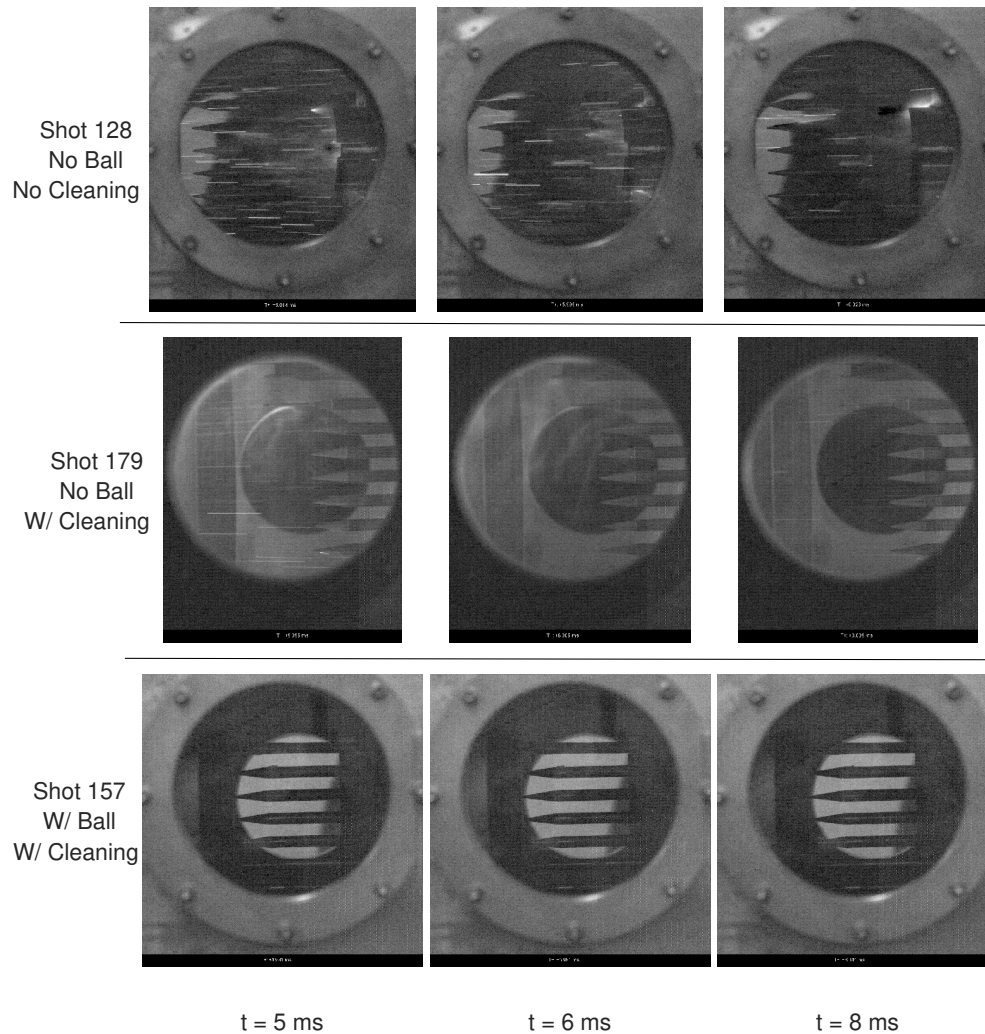
Fig. 10   Effect of Tunnel Cleaning Procedures and Centerbody Apparatus on Debris Entering the Test Section.

9
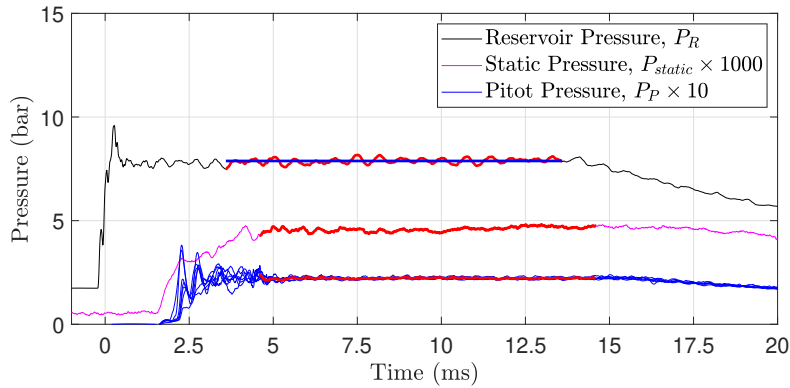
Fig. 11   Pressure Traces for Shot 173 with a 50% N$_2$/50% He Driver with $P_4/P_1 = 5$.

Table 3   Run Condition for a Shot with a Hollow-Cylinder Flare. P_4 is Driver-section pressure; P_4/P_1 is the driver-to-driven section ratio; u_s is the shock speed; M_s is the shock Mach number; T_r is the reservoir temperature; P_r is the reservoir pressure; h_r is the reservoir enthalpy; and Y/N denote yes or no, respectively. Ball and DD represent the use of a centerbody and double diaphragm, respectively.

Shot	P_4 (MPa)	P_4/P_1	u_s (m/s)	M_s	P_r (MPa)	T_r (K)	h_r (MJ/kg)	Ball	D. Loc.	DD
106	78.3	155	1325	3.81	5.55	1930	1.91	N	T	N

References

[1] Chu, R. S. M., Tsai, C. Y., and Bakos, R. J., "Driver gas contamination in a detonation-driven reflected-shock tunnel," *Shock Waves*, Vol. 13, 2004, pp. 367–380. doi: 10.1007/s00193-003-0221-2.

[2] Hornung, H. G., "Experimental Hypervelocity Flow Simulation, Needs, Achievements and Limitations," *Proceedings of the First Pacific International Conference on Aerospace Science and Technology*, Taiwan, 1993.

[3] Hannemann, K. and Schneider, M. and Reimann, B. and Schramm J. M., "The Influence and Delay of Driver Gas Contamination in HEG," *21^{s}t AIAA Aerodynamic Measurment Technology and Ground Testing Conference*, AIAA 2000-2593, Denver, Colorado, 2000, pp. 1–14. doi: 10.2514/6.2000-2593.

[4] Holden, M. S., "A Preliminary Study Associated with the Experimental Measurment of the Aero-optic Characteristics of Hypersonic Configurations," AD-A253 792, 1992.

[5] Holden, M. S., Wadhams, T. P., and Candler, G. V., "Experimental Studies in the LENS Shock Tunnel and Expansion Tunnel to Examine Real-Gas Effects in Hypervelocity Flows," *Proceedings of the 42nd AIAA Aerospace Sciences Meeting and Exhibit*, AIAA 2004-0916, Reno, Nevada, 2004. doi: 10.2514/6.2004-916.

[6] Holden, M. S., Wadhams, T. P., MacLean, M. G., and Dufrene, A., "Measurements in Regions of Shock Wave/Turbulent Boundary Layer Interaction from Mach 3 to 10 for Open and "Blind" Code Evaluation/Validation," AFRL-OSR-VA-TR-2013-0134, 2013.

[7] Sudani, N., and Hornung, H. G., "Gasdynamical Detectors of Driver Gas Contamination in a High-Enthalpy Shock Tunnel," *AIAA*, Vol. 36, No. 3, 1998, pp. 313–319. doi: 10.2514/2.383.

[8] Sudani, N., Valiferdowsi, B., and Hornung, H. G., "Test Time Increase by Delaying Driver Gas Contamination for Reflected Shock Tunnels," *AIAA*, Vol. 38, No. 9, 2000, pp. 1497–1503. doi: 10.2514/2.1138.

[9] Holden, M. S., "Development and Code Evaluation Studies in Hypervelocity Flows in the LENS Facility," *Proceedings of the 2nd European Symposium on Aerodynamics for Space Vehicles*, European Space Agency, ESTEC, Noordwijk, The Netherlands, 1994, pp. 319–334.
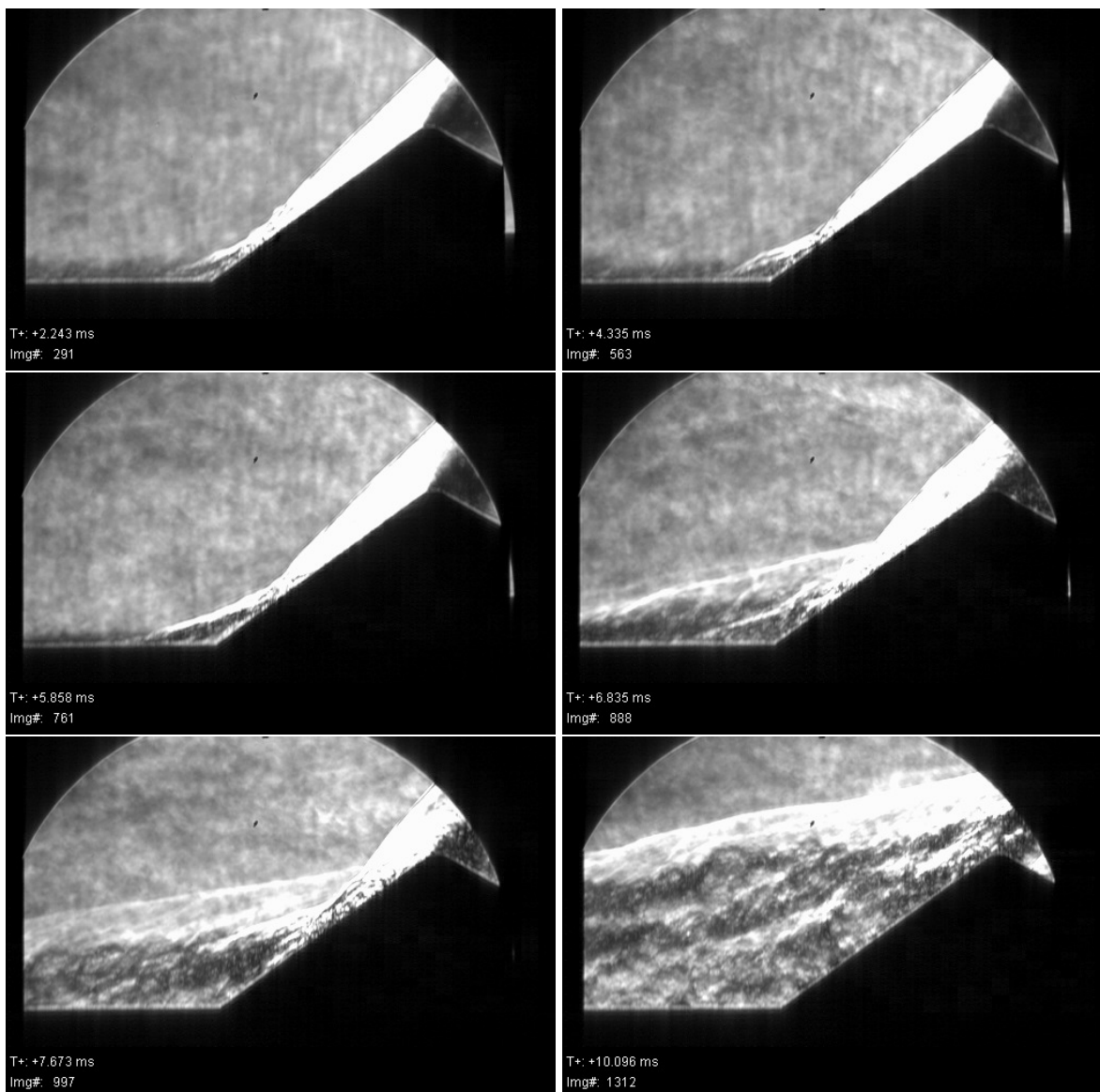
Fig. 12   Time-resolved Schlieren Imaging of a 36° Hollow-Cylinder Flare of 0.203 m (8 in) diameter for Shot 106. Note the size of the separation bubble is sensitive to the driver gas contamination.

[10] *ASME B16.5-2009 Pipe Flanges and Flanged Fittings: NPS 1/2 Through NPS 24 Metric/Inch Standard*, ASME, 2009.

[11] *ASME B31.1-2014 Power Piping: ASME Code for Pressure Piping, B31*, ASME, 2014.

[12] Gaydon, A. G., and Hurle, I. R., *The Shock Tube in High-Temperature Chemical Physics*, 1st ed., Reinhold Publishing Corporation, 1963.

[13] Goodwin, D. G., "An Open-Source, Extensible Software Suite for CVD Process Simulation," *Proceedings of CVD XVI and EuroCVD Fourteen, M Allendorf, F Maury, and F Teyssandier (Eds.)*, 2003, pp. 155–162.

[14] Browne, S., Ziegler, J., and Shepherd, J. E., "Numerical Solution Methods for Shock and Detonation Jump Conditions," GALCIT - FM2006-006, 2006.

[15] Gordon, S., and McBride, B., "Thermodynamic Data to 20000 K for Monatomic Gases," NASA TP-1999-208523, 1999.

[16] McBride, B. J., Zehe, M. J., and Gordon, S., "NASA Glenn Coefficients for Calculating Thermodynamic Properties of Individual Species," NASA TP-2002-211556, 2002.

11

[17] Wright, M. J., Candler, G. V., and Bose, D., "Data-Parallel Line Relaxation Method for the Navier-Stokes Equations," *AIAA Journal*, Vol. 36, No. 9, 1998, pp. 1603–1609. doi: 10.2514/2.586.

[18] Davies, L., "The Interaction of the Reflected Shock with the Boundary Layer in a Shock Tube. Part 1," Technical report, Her Majesty'S Stationary Office, Ministry of Aviation: Aeronautic Research Council, London, U.K., July 1966.

[19] Davies, L., and Wilson, J. L., "Influence of Reflected Shock and Boundary-Layer Interaction on Shock-Tube Flows," *Physics of Fluids*, Vol. 12, No. 5, 1969, p. I37. doi: 10.1063/1.1692625.

[20] Goozée, R. J., Seal, P. A., and Saxena, D. R., "Simulation of a complete reflected shock tunnel showing a vortex mechanism for flow contamination," *Springer Shock Waves*, Vol. 15, No. 3-4, 2006, pp. 165–176. doi: 10.1007/s00193-006-0015-4.

[21] Inc, I. S. S., "Fast Pressure Sensitive Paints," , 2021. URL https://innssi.com/fast-pressure-sensitive-paints/.

[22] Jewell, J. S., Parziale, N. J., Leyva, I. A., and Shepherd, J. E., "Effects of Shock-Tube Cleanliness on Hypersonic Boundary Layer Transition at High Enthalpy," *AIAA Journal*, Vol. 55, No. 1, 2017, pp. 332–338. doi: 10.2514/1.J054897.